Ozone Photolysis : strong isotopologue/isotopomer selectivity in the stratosphere

Steve Ndengué, Sasha Madronich, Fabien Gatti, Hans-Dieter Meyer, Rémy Jost, Ousmanou Motapon

AGU PUBLICATIONS

JGR

Journal of Geophysical Research: Atmospheres

RESEARCH ARTICLE
10.1002/2013JD020033

Key Points:
- Photolysis rate of various ozone isotopologues are calculated
- The ozone isotopic fractionation is determined versus altitude
- The role of three spectral bands of ozone is analyzed

Correspondence to:
R. Jost,
jost.remy.robert@gmail.com

Citation:
Ndengué, S., S. Madronich, F. Gatti, H.-D. Meyer, O. Motapon, and R. Jost (2014), Ozone photolysis: Strong isotopologue/isotopomer selectivity in the stratosphere, *J. Geophys. Res. Atmos.*, *119*, 4286–4302, doi:10.1002/2013JD020033.

Received 15 APR 2013
Accepted 18 JAN 2014
Accepted article online 25 JAN 2014
Published online 9 APR 2014

Ozone photolysis: Strong isotopologue/isotopomer selectivity in the stratosphere

Steve Ndengué[1,2], Sasha Madronich[3], Fabien Gatti[4], Hans-Dieter Meyer[5], Ousmanou Motapon[2], and Rémy Jost[1]

[1]Laboratoire Interdiciplinaire de Physique, Université Grenoble 1 / CNRS, UMR 5588, Grenoble, France, [2]Laboratoire de Physique Fondamentale, Université de Douala, Douala, Cameroon, [3]National Center for Atmospheric Research, Boulder, Colorado, USA, [4]CTMM, Institut Charles Gerhardt, UMR 5253, CC 1501, Université de Montpellier II, Montpellier, France, [5]Theoretische Chemie, Physikalisch-Chemisches Institut, Universität Heidelberg, Heidelberg, Germany

Abstract We calculated the photolysis rate coefficients of five ozone isotopologues/isotopomers as functions of altitude up to 80 km using recent ab initio absorption cross sections and an averaged actinic flux. Three of the five ozone isotopologues/isotopomers are symmetric, with a single isotopic dissociation channel, and two are asymmetric with two isotopic dissociation channels. The specific contributions of the Chappuis, Huggins, and Hartley bands to the photolysis rates and enrichments have been determined as a function of altitude. The Chappuis and Hartley bands have a dominant contribution to the photolysis rates, respectively at low and high altitudes, but these two bands are characterized by small fractionations. In contrast, the Huggins band has a minor contribution to the overall photolysis rate at any altitude, but it generates most of the strong fractionation which peaks around 35 km. The photolysis fractionations are "mass dependent" in contrast with those due to the ozone formation process which are "non–mass dependent." The altitude dependences of our photolysis fractionations are in qualitative agreement with those of Liang et al. (2006) but differ quantitatively, most notably because the contribution of the Huggins band has been reevaluated. The branching ratio between the two electronic dissociation channels (either $O(^3P)$ or $O(^1D)$ products) has been used to calculate the isotopic enrichments of the reactive $O(^1D)$ induced by ozone photolysis. The isotopic photolysis rates can be included in a global kinetic model that includes ozone formation processes and collision with O_2 and other oxygen-containing species.

1. Introduction

In the atmosphere, ozone molecules are continuously formed via the Chapman process [*Chapman*, 1930] and destroyed by photolysis or by chemical reactions [*Brasseur and Solomon*, 1984; *Warneck*, 1988]. The various ozone isotopologues and isotopomers (noted *abc*, see below) have slightly different absorption cross sections (hereafter noted $\sigma_{abc}(\tilde{\nu})$) which act on the isotopic oxygen budget of molecules with an odd number of oxygen atoms (O and O_3) and then, through chemical reactions and/or collision exchanges, on the oxygen isotope composition of other molecules like CO_2 [*Yung et al.*, 1997], SO_2, NO_2, N_2O [*Kaiser et al.*, 2004], and ClO_2.

The isotopic enrichments (the deviations from expected isotopic ratios at natural abundance) may be used to characterize or infer physical and chemical processes in the atmosphere. The two main origins of ozone enrichments are the ozone formation process [*Thiemens and Heidenreich*, 1983; *Mauersberger et al.*, 1989] and the ozone photolysis [*Liang et al.*, 2006; *Krankowsky et al.*, 2007]. Here we use the word of fractionation (instead of enrichment) to characterize the effect of the photolysis solely.

Until recently, the ozone enrichments observed in the stratosphere [*Mauersberger et al.*, 2001] have been mostly attributed to the ozone formation process because huge isotopic enrichments, up to ≈ 18%, have been observed in laboratory experiments [*Anderson et al.*, 1997, 1989]. These stratospheric and laboratory ozone enrichments are "non–mass dependent" [*Kaiser et al.*, 2004; *Mauersberger et al.*, 1989] in contrast with the ones due to photolysis which are expected to be "mass dependent" according to the theory [*Schinke*, 1993]. In the following, the expression non–mass dependent is preferred to the one of "mass independent." The contribution of the photolysis process to ozone enrichments was largely ignored or neglected until 2003, when *Chakraborty and Bhattacharya* [2003] made laboratory photolysis experiments and concluded that the photolysis is a non–mass-dependent process. However, *Cole and Boering* [2006] discarded this conclusion and showed that the ozone photolysis is mass dependent, in agreement with theory and with prediction

derived from ab initio calculations [*Ndengue et al*., 2010]. The contribution of ozone photolysis to the enrichments has been inferred both experimentally from the altitude dependence [*Haverd et al*., 2005; *Krankowsky et al*., 2007] and theoretically from the isotopologue/isotopomer dependence of the absorption cross sections [*Miller et al*., 2005; *Liang et al*., 2004]. In addition, *Shaheen et al*. [2007] studied the oxygen isotope ratios in various mixtures of O_2, O_3, and CO_2 irradiated with a Hg lamp and specifically identified the need for wavelength-dependent photolytic enhancements.

It is worth knowing that experimentally it is extremely difficult to isolate or synthesize a specific isotopologue/isotopomer of ozone (except $^{16}O_3$ and $^{18}O_3$) and then to record their specific absorption cross sections [*Dimitrov et al*., 1998]. In contrast, the various ozone isotopologues/isotopomers can be compared rather easily by quantum calculations. These calculations require the ozone potential energy surfaces (PESs) of the ground and low-lying electronic states [*Grebenshchikov et al*., 2007; *Schinke and McBane*, 2010]. These PESs are the same for all the isotopologues/isotopomers within the Born-Oppenheimer approximation and depend on the masses of the three oxygen isotopes being considered. The quality of these PESs is not of spectroscopic accuracy [*Ndengué et al*., 2010] but is sufficient to determine the isotopic dependence of the cross sections of various isotopologues/isotopomers, $\sigma_{abc}(\tilde{\nu})$. The imperfections of the ground state PES can be tested via a comparison of its (accurate) experimental vibrational frequencies with those determined by quantum calculations using the ab initio PESs which are off by few cm^{-1} [*Grebenshchikov et al*., 2007]. In contrast, the isotope shifts of these frequencies upon oxygen substitution are determined rather accurately, within only few tenths of cm^{-1}.

The short notation, *abc*, is used to designate the various ozone isotopologues. The letters *a*, *b*, and *c* can be either 6 for ^{16}O or 7 for ^{17}O or 8 for ^{18}O. At natural abundance, beside the main isotopologue, $^{16}O_3$ (noted 666), the four relevant ozone isotopologues/isotopomers are those having only one ^{18}O or one ^{17}O atom: $^{16}O^{18}O^{16}O$ (noted 686), $^{16}O_2{}^{18}O$ (668), $^{16}O^{17}O^{16}O$ (676) and $^{16}O_2{}^{17}O$ (667). The 686 and 676 species are "symmetric" (they belong to the C_{2v} symmetry group as does the 666), and the 668 and 667 are "asymmetric" (they belong to the C_s symmetry group). The other isotopologues/isotopomers are much rarer and have been ignored here.

The versatile Multiconfiguration Time-Dependent Hartree (MCTDH) method [*Meyer et al*., 2009], a wave packet propagation approach for the nuclear motion, has been used previously to determine the absorption cross sections, $\sigma_{abc}(\tilde{\nu})$, of the 18 ozone isotopologues in the range of the Hartley band (from ≈ 30,000 to ≈ 50,000 cm^{-1}) [*Ndengue et al*., 2010]. $\sigma_{abc}(\tilde{\nu})$ is expressed as a function of $\tilde{\nu}=1/\lambda$ which is the wavenumber, proportional to the photon energy, $\tilde{\nu} = E/hc$, expressed in cm^{-1}.

The $\sigma_{abc}(\tilde{\nu})$ of six ozone isotopologues have been calculated in the Huggins range ($\tilde{\nu}$ from ≈ 27,000 to ≈ 32,000 cm^{-1}) from the vibrational eigenstates and the Franck-Condon factors [*Ndengue et al*., 2012a]. We have also calculated $\sigma_{abc}(\tilde{\nu})$ in the range of the Chappuis band ($\tilde{\nu}$ from ≈ 12,000 to ≈ 26,000 cm^{-1}) with the MCTDH method [*Ndengue et al*., 2010] because the contribution of the Chappuis band to the absorption and to the ozone photolysis is significant at "medium" altitudes (≈ 24–40 km) and dominant at "low" altitude, below ≈ 24 km (see below). This may be surprising because the maximum of $\sigma_{abc}(\tilde{\nu})$ in the range of the Hartley band, near 40,000 cm^{-1}, is a thousand times stronger than the one of $\sigma_{abc}(\tilde{\nu})$ in the range of the Chappuis band, near 16,000 cm^{-1}. However, below 24 km, the actinic flux in the range of the Hartley band is almost fully absorbed by the stratospheric ozone layer, so that the contribution of the Hartley band to the photolysis rate is weak at low altitudes (see section 2).

Globally, the Chappuis, Huggins, and Hartley bands of ozone included in our calculations cover the whole visible-UV range from 12,000 cm^{-1} to 50,000 cm^{-1}. Only the much weaker contribution of the Wulf bands, below 12,000 cm^{-1}, has been neglected.

Beside the isotopic distribution of the O_2 and O dissociation products, the oxygen atom can be formed either in a triplet state ($O_3 \rightarrow O_2\ (^3\Sigma) + O\ (^3P)$) or in a singlet state: $O_3 \rightarrow O\ (^1D) + O_2\ (^1\Delta)$. In short, the electronic branching ratio favors the singlet channel (≈ 90%) at energy above ≈ 32,000 cm^{-1}, while only the triplet channel is energetically open at lower energies. The branching ratios (hereafter noted ϕ) between the various electronic and isotopic dissociation channels have been determined with the MCTDH code for the five isotopologues of ozone [*Ndengue et al*., 2012b].

The results presented in our three previous papers [*Ndengue et al*., 2010, 2012a, 2012b] deal only with the ozone cross-section isotope shifts and are independent of any light source. In contrast, the present paper

deals with the fractionations and enrichments corresponding to the actinic flux presented in section 2 which is averaged and depends only on $\tilde{\nu}$ and on the altitude, h. Fractionations and enrichments for specific actinic fluxes can be obtained with our cross sections.

In 2006, *Liang et al*. [2006] built a kinetic model predicting various isotopic enrichments due to ozone formation, ozone photolysis, and collision isotope exchanges. Three approximations used by Liang et al. in their calculation of the contribution of the photolysis to the enrichments (here this contribution solely is named fractionation) have been improved, owing to the results presented in three previous papers, and are detailed below in section 4.1.1. The oxygen isotopic and electronic fractionations due to the ozone photolysis depend strongly on the energy spectrum of the actinic flux (hereafter noted S), which varies strongly with altitude. In this paper, we have calculated an actinic flux averaged over latitude, season, and time and considered only its altitude dependence. However, the latitude dependence of the photolysis rates (and then of the related fractionations) may be approximately converted into an altitude rescaling (see below, Figure 4). We have also calculated the corresponding oxygen isotopic and electronic fractionations due solely to the photolysis process for the five ozone isotopologues. These calculated isotopologue fractionations are given for altitudes between 0 and 80 km by steps of 4, 8, or 10 km depending on to the altitude.

Our calculated fractionations due to the photolysis process are partial in the sense that they do not take into account the contribution of the ozone formation process, which induces other fractionations with a specific altitude dependence which differ from the one of the photolysis process. The present contribution of the ozone photolysis can be included in a global model including the ozone formation process and the destruction of ozone by O_x, Cl_x, Br_x, NO_x, HO_x, ClO_x, and BrO_x.

The paper is organized as follows: section 2 presents a description of the ozone layer and of the actinic flux; section 3 is devoted to the photolysis rates of five relevant ozone isotopologues/isotopomers; section 4 presents the altitude dependences of the odd oxygen (O and O_3) isotopic fractionations and of the $O(^1D)/O(^3P)$ ratio; section 5 gives some conclusions and perspectives.

2. The Ozone Layer and the Actinic Flux Altitude Dependence

The ozone photolysis process is induced by the actinic flux, $S(\lambda, h)$ or $S(\tilde{\nu}, h)$, that strongly depends on altitude, h, and on $\tilde{\nu}$. At a given altitude, the actinic flux is mainly dependent on the ozone column lying above this altitude. In other words, the ozone layer is both an optical filter for the actinic flux and also the "sample" that we are studying. The actinic flux spectrum was calculated using the Tropospheric Ultraviolet-Visible (TUV) model version 5 [*Madronich and Weller*, 1990]. The model simulates the propagation of solar radiation through the atmosphere, accounting for Rayleigh scattering by N_2 and O_2 molecules and absorption by O_2 and O_3. The vertical profiles for air density, temperature, and O_3 were taken from the *U.S. Standard Atmosphere* [1976], over 0–80 km in 1 km layers, with no clouds, aerosols, or other gaseous absorbers and a surface albedo of 10%. Ozone concentrations were rescaled by the ratio of climatological column values (by month and latitude, from [*Fortuin and Kelder*, 1998]) to the U.S. Standard Atmosphere value of 349 Dobson units.

The reference solar spectrum of *Chance and Kurucz* [2010] was used over 200–1000 nm, with a resolution of 0.04 nm full width at half maximum sampled at 0.01 nm. Ozone absorption cross sections for the Hartley and Huggins bands were from *Malicet et al*. [1995] and for the Chappuis band from *Brion et al*. [1998], both available at 0.01 nm resolution. Usually, the use of such high-resolution data is not necessary for calculation of photolysis coefficients [*Madronich and Weller*, 1990], but here it was deemed useful because of the relatively small spectral shifts among the various $\sigma_{abc}(\tilde{\nu})$ and the importance of correct overlap with structures in the solar spectrum (e.g., Fraunhofer lines). The initial actinic flux given as a function of λ was converted into an actinic flux depending on $\tilde{\nu}$ because our $\sigma_{abc}(\tilde{\nu})$ are expressed as a function of $\tilde{\nu}$. Interpolation to the 10 cm^{-1} computational and output grid used in the model was done with a simple trapezoidal algorithm.

The TUV model provides the number of solar photons (quanta $cm^{-2}\,s^{-1}\,cm^{-1}$) at a specific time, altitude, and latitude. The calculation of the spectrum was repeated for 17 latitude bands, each having a width of 10°, centered from 80°S to 80°N, using 15 min time steps for the fifteenth day of each month. These values were then averaged over the 12 months to obtain the actinic flux as a function of latitude and altitude. Averaging over latitudes was done with area-weighting to obtain $S(\tilde{\nu}, h)$, an annually averaged actinic flux as a function of altitude.

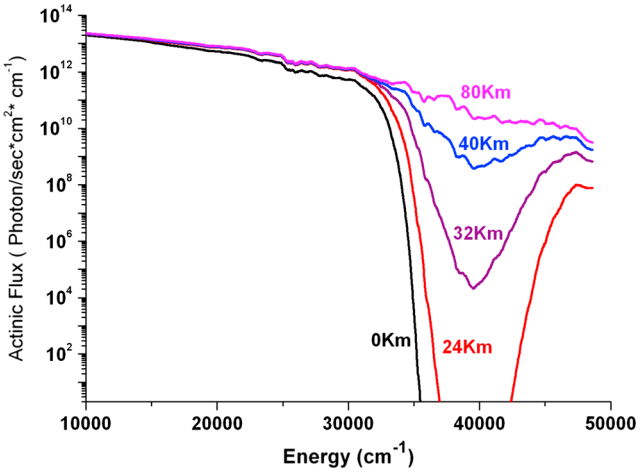

Figure 1. Energy dependence of the actinic flux (log scale) for five representative altitudes. The actinic flux at 0 km is very weak (off scale) for photon energies larger than 35,000 cm^{-1}. At higher energies, above 50,000 cm^{-1}, the absorption by N_2 and O_2 is dominant and the actinic flux is negligible. In the range below 30,000 cm^{-1}, the decrease of the actinic flux at an altitude of 0 km (compared with the ones at higher altitudes) is mostly due to light scattering by N_2 and O_2.

The use of an averaged actinic flux allows us to focus on the altitude dependence of the enrichments. More specific enrichments corresponding to local and/or temporal situations can be obtained by using the relevant actinic flux and the set of $\sigma_{abc}(\tilde{\nu})$ and ϕ which are used below.

In sections 3 and 4, the various calculations have been performed with $S(\tilde{\nu}, h)$ determined every 4 km between 0 and 80 km. Figure 1 shows the averaged actinic flux plotted versus photon energy (in cm^{-1}) for five representative altitudes of 0, 24, 32, 40, and 80 km.

In Figure 1, the extraordinary strong decrease (by numerous orders of magnitude) of the actinic flux around 40,000 cm^{-1} is due to the absorption by ozone molecules lying above each given altitude, in the range of the Hartley band. In contrast, the much smaller decrease due to absorption in the range of the Chappuis band near 20,000 cm^{-1} is too weak to be seen with the logarithmic scale of Figure 1. Consequently, the photolysis rates of the various ozone isotopologues/isotopomers are also strongly dependent on the altitude (see below, Figures 3 and 4).

3. Photolysis Rates of Five Ozone Isotopologues/Isotopomers

The photolysis rate coefficient [*Brasseur and Solomon*, 1984; *Warneck*, 1988],

$$J_{abc}(h) = \int \sigma_{abc}(\tilde{\nu}) S(\tilde{\nu}, h) \mathrm{d}\tilde{\nu}. \quad (1a)$$

An equivalent formula replacing $\tilde{\nu}$ by λ is often used. In this paper, we assume that each photoexcited ozone molecule dissociates (and then no collisional relaxation to the ground state occurs). Otherwise, a distinction between photoexcitation and photodissociation cross sections is not required.

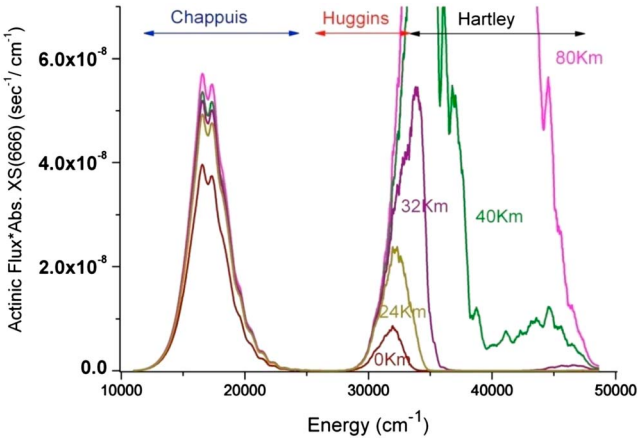

Figure 2. Contributions to ozone photolysis from different spectral regions, showing the product $\sigma_{666}(\tilde{\nu})\ S(\tilde{\nu},h)$ as a function of $\tilde{\nu}$, for five altitudes of 0, 24, 32, 40, and 80 km (see text and Figure 1). The corresponding products for the four other isotopologues/isotopomers are very similar and are not shown.

The integration over $\tilde{\nu}$ (or over λ) can be performed either on the whole visible-UV range (here from 12,500 to 50,000 cm^{-1}) or on reduced energy ranges like those corresponding to the Chappuis, Huggins, and Hartley bands. The contribution of the Chappuis band to the total photolysis rate, $J_{abc}^{\text{Chappuis}}(h)$ corresponding to the energy range of $\{l = 12{,}500\ cm^{-1}, u = 26{,}000\ cm^{-1}\}$, is as follows:

$$J_{abc}^{\text{Chappuis}}(h) = \int_{l}^{u} \sigma_{abc}(\tilde{\nu}) S(\tilde{\nu}, h) \mathrm{d}\tilde{\nu}. \quad (1b)$$

Two similar expressions (not written) exist for $J_{abc}^{\text{Huggins}}(h)$, with $\{l = 26{,}000\ cm^{-1}, u = 33{,}000\ cm^{-1}\}$ and for $J_{abc}^{\text{Hartley}}(h)$ with $\{l = 33{,}000\ cm^{-1}, u = 50{,}000\ cm^{-1}\}$, the

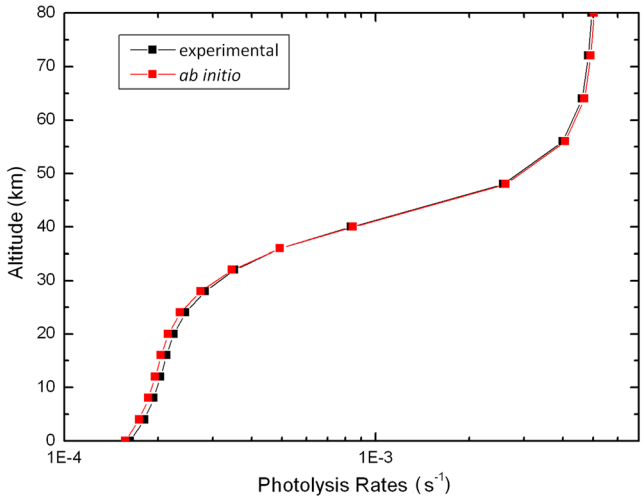

Figure 3. Comparison between two $J_{666}(h)$ photolysis rates obtained either with the calculated (ab initio) or with the experimental $\sigma_{666}(\tilde{\nu})$. Above 56 km, there is a small overestimation of the ab initio $J_{666}(h)$ because the ab initio $\sigma_{666}(\tilde{\nu})$ is slightly overestimated in the highest energy range. This $\sigma_{666}(\tilde{\nu})$ overestimation is in turn due to a small imperfection of the potential energy surface used to calculate $\sigma_{666}(\tilde{\nu})$.

sum of the three being equal to $J_{abc}(h)$. We can also define the relative contributions of the three bands to the $J_{abc}(h)$, as (e.g., for the Chappuis band):

$$F_{abc}^{\text{Chappuis}}(h) = J_{abc}^{\text{Chappuis}}(h)/J_{abc}(h). \quad (1c)$$

Below we describe the strong altitude dependence of the photolysis rate of the 666 isotopologue, which is taken as a reference. The altitude dependence of the photolysis rates is strongly related to the altitude dependence of the product of $\sigma_{abc}(\tilde{\nu})\ S(\tilde{\nu}, h)$, which is shown in Figure 2, for the 666 isotopologue and for the five altitudes used in Figure 1.

Figure 2 shows that the contribution of the Hartley band to the total $J_{666}(h)$ is dominant at altitudes above 32 km and decreases by several orders of magnitude with decreasing altitudes. This huge reduction is due to the screening effect by ozone molecules present in the layers located above the considered altitude (see Figure 1). Below ~32 km, the contribution of the Hartley band is restricted to its low-energy wing, which is named the Huggins band. In contrast, the Chappuis band contribution to the photolysis rate is almost independent of altitude. The corresponding plots for the other isotopologues/isotopomers are very similar and not shown.

A comparison of the photolysis rates calculated with the same actinic flux but either with the calculated or with the experimental $\sigma_{666}(\tilde{\nu})$ is shown in Figure 3. Moreover, our calculated photolysis rate of 0.0051 s^{-1} at 80 km is in reasonable agreement with the value of 0.0046 s^{-1} (at 130 km) used by *Liang et al.* [2006], the tiny difference between the two being mainly due to a choice of a slightly different averaged actinic flux.

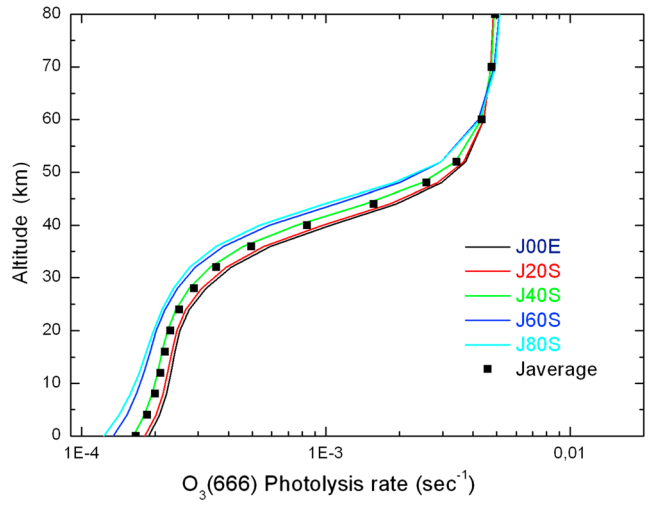

Figure 4. Altitude dependence of the annually averaged 666 photolysis rate for five latitudes (0°, 20°, 40°, 60°, and 80°) of the Southern Hemisphere and the cosine weighted average (black square) which is also shown in Figure 3. The Northern Hemisphere dependence (not shown) is very similar. The other isotopologues have very similar altitude and latitude dependences.

The altitude dependences of photolysis rates of the 667, 668, 676, and 686 ozone isotopologues/isotopomers, integrated from 12,500 to 50,000 cm^{-1}, are very similar to the one of 666 (Figure 3) and are not shown. The tiny differences between the photolysis rates of these five isotopologues are in the following order: $J_{666} > J_{667} > J_{668} > J_{676} > J_{686}$. Because the photolysis is a destruction process, a smaller photolysis rate for a given isotopologue implies a larger remaining fraction of this isotopologue. It is interesting to note that this hierarchy of $J_{abc}(h)$ is different from the one of the formation process, which favors the formation of the asymmetric isotopologues more than the symmetric ones

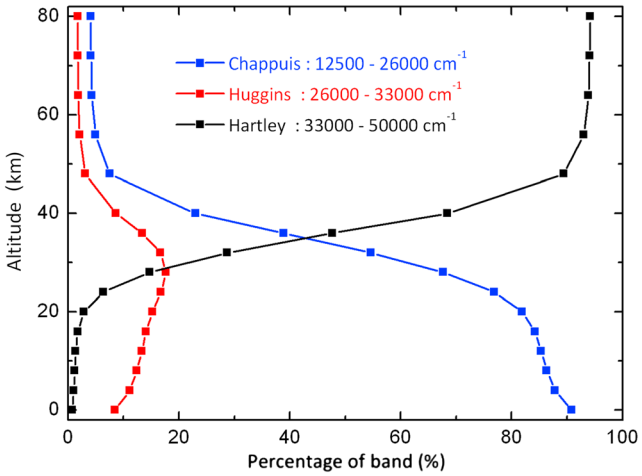

Figure 5. Altitude dependence of the relative contributions (in %) of the Chappuis, Huggins, and Hartley bands to $J_{666}(h)$, the total photolysis rate of $^{16}O_3$. The figures for the other isotopologues/isotopomers (not shown) are very similar.

[*Mauersberger et al.*, 1989]. Globally, both the photolysis and the formation processes favor the rare isotopologues (when 666 is taken as a reference) but in different ways: the formation process favors the formation of asymmetric species, 667 and 668, and is non–mass dependent, while the photolysis process favors (dissociates less efficiently) the symmetric species, 676 and 686, and is mass dependent.

In order to estimate the latitude dependence of $J_{666}(h)$, we plotted in Figure 4 the altitude dependence of annually averaged photolysis rates for five latitudes.

Above ~60 km, the photolysis rate is almost independent of latitude because the actinic flux is weakly absorbed by the remaining overhead ozone. In contrast, the latitude dependence of photolysis coefficients increases significantly at lower altitude, the photolysis rate being about twice higher near the equator than near the South Pole. Note that a latitude shift can be converted approximately into an altitude shift (or rescaling).

Below we analyze the relative contributions of the three spectral ranges corresponding to the three bands (Chappuis, Huggins, and Hartley) to $J_{abc}(h)$, and we show that these contributions are strongly dependent on the altitude. Figure 5 shows these relative contributions of the Chappuis, Huggins, and Hartley bands only for $J_{666}(h)$ because the contributions for other $J_{abc}(h)$ are very similar. Our two boundaries of 26,000 cm^{-1} and 33,000 cm^{-1} are more or less arbitrary (within ± 1000 cm^{-1}), but the results shown in Figure 5 and below do not depend significantly on these boundaries.

Three ranges of altitudes can be qualitatively distinguished in Figures 3, 4, and 5:

1. Above ~60 km, the actinic flux is weakly absorbed by uppermost ozone, and the large photolysis rate is mostly due to the contribution of the Hartley band.
2. Between ~60 km and ~30 km the photolysis rate decreases abruptly by about a factor 25 because the contribution of the Hartley band decreases enormously. In this range, the contribution of the Huggins band decreases in absolute value (Figure 2) but its relative contribution (Figure 5) increases significantly. In this 60 to 30 km altitude range, the contribution of the Chappuis band is almost unchanged (see Figure 2) but its relative contribution (Figure 5) increases significantly.
3. Below ~24 km the photolysis rate is weakly dependent on the altitude because the photolysis contribution of the Chappuis band is dominant, even if it contribution to the enrichments is weak (see section 4.1 below). In contrast, the Huggins band has a much weaker photolysis contribution but a dominant enrichment contribution, as shown below in Figures 6 and 7.

Around 25 to 35 km, the relative contribution of the Huggins band (see Figure 5) reaches its maximum, explaining the strong enrichments displayed below in Figures 6 and 7 in this altitude range.

In summary, the Hartley, Huggins, and Chappuis bands play different roles on both the overall photolysis rates presented above (Figure 4) and on the isotopologue fractionations (and then enrichments) presented in the next section, both varying dramatically in the altitude range from ≈ 20 to ≈ 50 km corresponding to the denser part of the ozone layer which strongly absorbs the solar flux in the UV (see Figure 1).

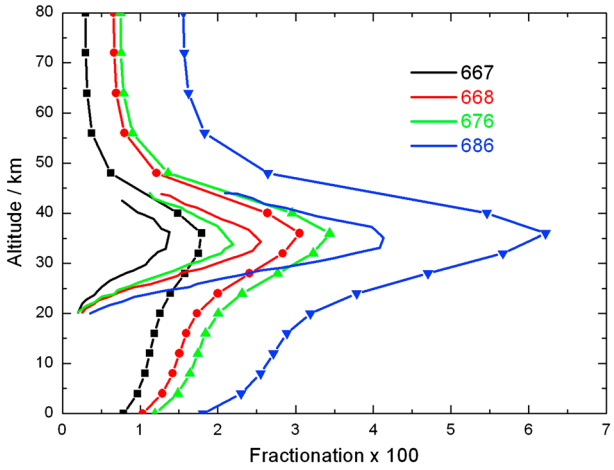

Figure 6. Comparison of the altitude dependence of our calculated photolysis fractionations (in %, thick lines with square markers) with those of Liang (thick lines without markers) [*Liang et al.*, 2006]. The colors correspond to the various isotopologues/isotopomers: 667 (black), 676(green), 686(blue), and 668(red). Our hierarchy between the 676 and 668 isotopologues is inverted from the one of Liang. The photolysis fractionations of Liang are given only in the altitude range between 20 and 44 km. The contribution of the Huggins band (between 27,000 and 31,250 cm^{-1}) is included in our photolysis fractionations while it has been neglected by Liang et al.

4. The Altitude Dependence of the Fractionations and of the Branching Ratios Relevant for the Production of Odd Oxygen, O, and O_3

Two types of fractionations are presented: In section 4.1, the isotopic fractionations due to the difference between the photolysis rates of the various species relative to the one of the 666 isotopologue; and in section 4.2, the atomic oxygen isotopic fractionations due to the two dissociation channels of the asymmetric isotopologues. These oxygen atomic fractionations are related to the branching ratio between the two electronic channels, $O(^1D)$ versus $O(^3P)$. These various types of fractionations take into account here only the photolysis process and do not consider other processes like the well-known ozone formation process [*Mauersberger et al.*, 1981; *Thiemens and Heidenreich*, 1983]. The fractionations presented below show how the photolysis process acts on the isotopic compositions of O_3 and O as a function of altitude.

Here it is timely to relate the concept of cross-section fractionation used in our previous papers [*Ndengue et al.*, 2010, 2012a, 2012b] with the one of photolysis fractionation used below: $f_{abc}(\tilde{\nu})$, the cross-section fractionation for an isotopologue *abc*, can be defined as follows: $f_{abc}(\tilde{\nu}) = \{[\sigma_{abc}(\tilde{\nu})/\sigma_{666}(\tilde{\nu})] - 1\}$ (in % or ‰). Here we use the reduced energy $\tilde{\nu}$ as variable, but the wavelength can be used as well. A fractionation, $f_{abc}(\tilde{\nu})$, can be averaged over any reduced energy range. In contrast, a photolysis fractionation is defined for a specific spectral source (here the altitude dependent actinic flux), and it can be integrated over any reduced energy range (equation (1a)) or wavelength range (equation (1b)). A large photolysis fractionation can be obtained only for a large cross-section fractionation and a large actinic flux occurring at the same energy (or spectral) range.

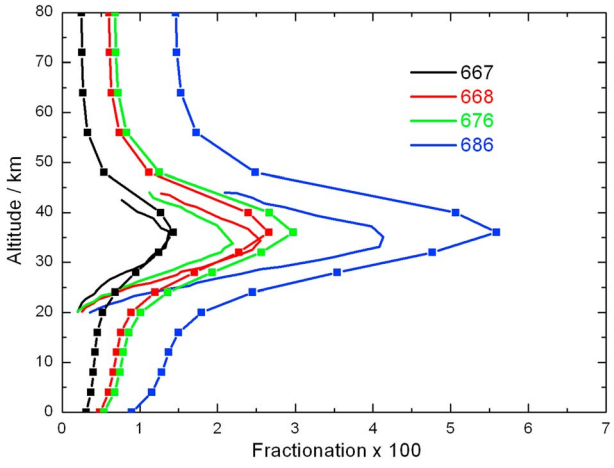

Figure 7. Comparison of the altitude dependence of our calculated fractionations (in %, thick lines with square markers) when the contribution of the Huggins band below 31,250 cm^{-1} is neglected with those of Liang (thick lines without markers) [*Liang et al.*, 2006]. The colors correspond to the various ozone species: 667 (black), 676 (green), 686 (blue), and 668 (red). As for Figure 6, our hierarchy between the 676 and 668 isotopologues is inverted from the one of Liang (see text for a detailed comparison between Figures 6 and 7).

4.1. Ozone Isotopologues/Isotopomers Fractionations Due to Photolysis

The photolysis fractionation of an *abc* isotopologue (see section 3) is defined as follows:

$$\varepsilon_{abc}(h) = -((J_{abc}(h)/J_{666}(h)) - 1). \quad (2)$$

There is a front minus sign in this equation because ozone photolysis is a destruction process. The photolysis fractionations obtained with equation (2) can be interpreted as a sum of contributions corresponding to various spectral ranges. For ozone, the three relevant spectral

ranges are those of the bands of Chappuis (12,500–26,000 cm^{-1}), Huggins (26,000–33,000 cm^{-1}), and Hartley (33,000–50,000 cm^{-1}) already used for Figures 1, 2, and 5. The $J_{abc}(h)$ photolysis rates can be divided according to these three bands, and partial photolysis fractionations can be defined (e.g., for the Chappuis band) as follows:

$$\varepsilon_{abc}^{\text{Chappuis}}(h) = -\left(\left(J_{abc}^{\text{Chappuis}}(h)/J_{666}^{\text{Chappuis}}(h)\right) - 1\right) \tag{2a}$$

and two similar expressions for $\varepsilon_{abc}^{\text{Huggins}}(h)$ and $\varepsilon_{abc}^{\text{Hartley}}(h)$.

The global photolysis fractionation, $\varepsilon_{abc}(h)$, can be expressed as a sum of the contributions of the three bands, weighted according to their relative contributions to $J_{666}(h)$: $F_{abc}^{\text{Chappuis}}(h)$, $F_{abc}^{\text{Huggins}}(h)$, and $F_{abc}^{\text{Hartley}}(h)$:

$$\varepsilon_{abc}(h) = \varepsilon_{abc}^{\text{Chappuis}}(h)F_{abc}^{\text{Chappuis}}(h) + \varepsilon_{abc}^{\text{Huggins}}(h)F_{abc}^{\text{Huggins}}(h) + \varepsilon_{abc}^{\text{Hartley}}(h)F_{abc}^{\text{Hartley}}(h). \tag{3}$$

Our photolysis fractionations are shown in Figure 6 (line + symbols), for altitudes between 0 and 80 km, for the four main isotopologues. The photolysis fractionations (named enrichments by Liang) obtained previously by *Liang et al*. [2006] between 20 and 44 km (full lines) are shown for comparison. A detailed comparison between these two sets of photolysis fractionations is presented in section 4.1.1.

The four main characteristics of the photolysis fractionations presented in Figure 6 are the following:

1. The peaks of photolysis fractionations occurring around 35 km are mostly due to the contribution of the Huggins band (see Figure 5), which contributes less than 20% of the photolysis rate but which has a cross-section fractionation factor much larger than the ones of the Hartley and Chappuis bands [see *Ndengue et al*., 2010, Figure 4].
2. The isotopologue hierarchy of photolysis fractionation is the same at all altitudes.
3. The photolysis fractionations for the two symmetric isotopomers, 676 and 686, are about 50% higher than for the two corresponding asymmetric isotopomers, 667 and 668. The photolysis process favors the symmetric isotopomers (they are less photolyzed), while the ozone formation process favors the formation of asymmetric isotopomers [*Mauersberger*, 1999], the latter being dominant.
4. The comparison between ozone species with one ^{17}O and those with one ^{18}O shows that the photolysis process has a mass-dependent character, which contrasts with the non–mass-dependent character of the formation process [*Thiemens and Heidenreich*, 1983; *Hathorn and Marcus*, 1999].

4.1.1. Comparison With Results of Liang et al. (2006)

Our photolysis fractionations displayed in Figure 6 are in qualitative but not quantitative agreement with those of *Liang et al*. [2006, Figure 7, dashed lines]. Around 35 km, our 676 and 686 fractionations are about 50 % higher than those of Liang et al., while, for 667 and 668, they are only 20% higher. This difference between symmetric and asymmetric isotopologues is discussed below. Around 20 km, our fractionations are several times higher than those of Liang et al. The three main differences between the calculations by Liang et al. and the ones presented above are as follows: (i) the isotopic dependences of the various $\sigma_{abc}(\tilde{\nu})$ have been obtained by *Liang et al*. [2004] with an analytic model, while the ones used here have been calculated with a full quantum mechanical approach using the MCTDH code [*Ndengue et al*., 2010] (the differences between the two are discussed below); (ii) the contribution to the photolysis rates of the Huggins band between 27,000 and 31,250 cm^{-1}, which has been neglected by *Liang et al*. [2006], has been taken into account in our calculations; (iii) the isotopic branching ratios, ϕ, between the two dissociation channels of the 667 and 668 asymmetric isotopologues, assumed to be 0.5 by Liang, have been determined with the same MCTDH code [*Ndengue et al*., 2012b]. To quantify the contribution of the Huggins range between 27,000 and 31,250 cm^{-1}, we have calculated the enrichments when this range is excluded which are plotted in Figure 7.

The contribution of the 27,000–31,250 cm^{-1} range (the low-energy part of the Huggins band) to the fractionations can be estimated from a comparison of Figures 6 and 7. This contribution increases smoothly, from almost 0% at 80 km to about 50% at low altitudes for the four isotopologues/isotopomers. Around 35 km, the fractionations for the 686 isotopologue are respectively of 6.4% (in Figure 6) and 5.7% (in Figure 7). This change may be surprising since the contribution of the 27,000–31,250 cm^{-1} energy range is only 2% of the overall photolysis rate at 35 km (see Figure 2), but this energy range has a large cross-section fractionation factor, $f_{abc}(\tilde{\nu})$, which explains its large contribution to the photolysis fractionation [see *Ndengue et al*., 2010,

Figure 4; *Ndengue et al*., 2012b, Figures 7 and 8; *Miller et al*., 2005, Figures 1 and 2]. At 20 km, a similar comparison shows that the 27,000–31,250 cm^{-1} range contributes about 40% of the fractionation: e.g., for the 686 isotopologue, the fractionations are respectively of 3.2% in Figure 6 and only 1.8% in Figure 7.

Another striking difference between our fractionations and those of Liang et al. is on the ratios between the symmetric (676 or 686) and the asymmetric (667 or 668) isotopomers: these ratios are about 2 in our results (Figure 6) and only about 1.6 in those of *Liang et al*. [2006]. This difference of fractionation ratios originates from the $\sigma_{abc}(\tilde{\nu})$ dependence to either a central (e.g., 686) or to a lateral (e.g., 668) isotopic substitution. In their analytic model, Liang et al. [*Liang*, 2004] assume that the (tiny) change of the $\sigma_{abc}(\tilde{\nu})$ cross sections under isotopic substitution is proportional to the corresponding (tiny) change of the zero point energy (ZPE) for both a central and a lateral substitution. This assumption has been discussed in the case of the Hartley band calculated by *Ndengue et al*. [2010]. These calculated numerical cross sections, $\sigma_{abc}(\tilde{\nu})$, have been fitted with an analytic model using four parameters: amplitude, center, width, and asymmetry. This asymmetry parameter, which plays a role similar to the $\gamma(V_0, E)$ function used by Liang et al. [see *Liang et al*., 2004, equations 7 and 9], is not constant (as assumed by Liang et al. for $\gamma(V_0, E)$) nor vary like the ZPE under an isotopic substitution as assumed by Liang et al. for the three other parameters. As a consequence of the asymmetry parameters, the fractionation hierarchy is inverted from the one of Liang et al.: the 676 isotopologue has a larger cross-section fractionation than the one of 668 below 37,000 cm^{-1}. This result explains why, in Figures 6 and 7, the 676 photolysis fractionation due to the actinic flux is higher than the one of the 668 at any altitude, in contrast with the results of Liang et al. We have checked that the $\sigma_{abc}(\tilde{\nu})$ temperature dependence has a minor impact on the fractionations and then on their altitude dependences. *Liang et al*. [2006] have drawn the same conclusion.

4.2. Atomic Oxygen Fractionations

Due to the low dissociation energy threshold of ozone at about 1.05 eV (8500 cm^{-1}) [*Grebenschikov*, 2007], each photon of energy $>$ 1.05 eV can induce the dissociation of ozone into $O_2 + O$. Radiation and/or collisional processes may stabilize the excited ozone and avoid dissociation, but these processes will be neglected here.

The three oxygen atoms channel ($O_3 \rightarrow O + O + O$) being not energetically accessible, at least for $\tilde{\nu}$ lower than ~47,600 cm^{-1}, the three symmetric species (666, 676, and 686) have a single dissociation channel ($O_3 \rightarrow O_2 + O$) with a unique isotopic distribution because the central oxygen atom of ozone belongs always to the molecular oxygen product and is never the atomic oxygen product. This occurs because the barrier to permute the central oxygen with one of the two lateral oxygen atoms is too high. In contrast, the asymmetric isotopomers (667 and 668) have two nondegenerate dissociation channels corresponding to two isotopes distributions: e.g., the 668 can dissociate either into 66 + 8 or into 68 + 6, the later channel being slightly favored because the ZPE of 68 ($^{16}O^{18}O$) is lower than the one of 66 ($^{16}O^{16}O$) and its dissociation energy threshold is slightly lower. These two isotopic dissociation channels, 66 + 8 and 68 + 6, have slightly different probabilities and then unequal branching ratios, which contribute to the atomic oxygen and ozone isotopic enrichments [*Ndengue et al*., 2012b].

According to its isotopic composition, the photolysis of an ozone molecule may lead to either two (two electronic) or four (two electronic times two isotopic) dissociation channels, each being characterized by its photolysis rate. The overall photolysis rate of an *abc* isotopologue may split into four rates:

$$J_{abc}(h) = J_{abc}\left(ab + c\left(^1\mathrm{D}\right); h\right) + J_{abc}\left(ab + c\left(^3\mathrm{P}\right); h\right) + J_{abc}\left(bc + a\left(^1\mathrm{D}\right); h\right) + J_{abc}\left(bc + a\left(^3\mathrm{P}\right); h\right). \quad (4)$$

These four photolysis rates can be grouped two by two, either according to the isotopic composition of the O_2 product (whatever the electronic state of the O atom; see section 4.2.1) or according to the electronic state of the O atom (whatever the isotopic composition of O_2; see section 4.2.2). However, for other specific processes, like the atomic oxygen collision exchange with CO_2, the two relevant photolysis rates, associated to the production of either $^{17}O(^1D)$ or $^{18}O(^1D)$, are the $J_{667}(h)$ $(66 + 7(^1D); h)$ and the $J_{668}(h)$ $(66 + 8(^1D); h)$ which can be obtained from the results presented below (sections 4.2.1 and 4.2.2).

4.2.1. Isotope Atomic Oxygen Enrichments

In this section we determine the isotopic enrichments of the atomic oxygen product for various isotopologues and isotopomers of ozone. The 666, 686, and 676 symmetric isotopologues have a single

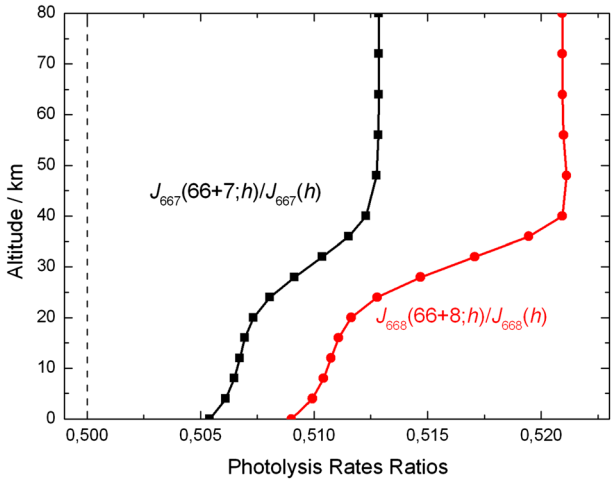

Figure 8. Photolysis branching ratios between the two dissociation channels of 667 and 668 asymmetric isotopologues. A ratio of 0.500 corresponds to an equal probability for the two isotopic dissociation channels given above by equations (7a) and (7b) and equations (8a) and (8b), respectively for the 667 and 668 isotopologues.

photodissociation channel because the central atom of ozone belongs to the molecular oxygen dissociation product:

$$666 + h\upsilon \rightarrow 66 + 6 \quad (5)$$

$$676 + h\upsilon \rightarrow 67 + 6 \quad (6)$$

$$686 + h\upsilon \rightarrow 68 + 6. \quad (7)$$

Then, these three symmetric isotopologues, 666, 676, and 686, always liberate an ^{16}O atom when they are photolyzed with a photon of frequency υ (or of wavenumber $\tilde{\nu} = \upsilon/c$).

In contrast, the two asymmetric isotopologues, 667 and 668, have two nondegenerate isotopic dissociation channels which are given with their corresponding branching ratios:

$$667 + h\upsilon \rightarrow 66 + 7 \qquad \phi_{667}(66 + 7; \tilde{\nu}) \quad (7a)$$

$$667 + h\upsilon \rightarrow 67 + 6 \qquad \phi_{667}(67 + 6; \tilde{\nu}) \quad (7b)$$

$$668 + h\upsilon \rightarrow 66 + 8 \qquad \phi_{668}(66 + 8; \tilde{\nu}) \quad (8a)$$

$$668 + h\upsilon \rightarrow 68 + 6 \qquad \phi_{668}(68 + 6; \tilde{\nu}). \quad (8b)$$

These branching ratios obey $\phi_{667}(66+7;\tilde{\nu}) + \phi_{667}(67+6;\tilde{\nu}) = 1$ and $\phi_{668}(66+8;\tilde{\nu}) + \phi_{668}(68+6;\tilde{\nu}) = 1$. These branching ratios, calculated recently [*Ndengue et al.*, 2012b], show that the photolysis of the 667 isotopologue favors slightly channel 7b with $\phi_{667}(67+6;\tilde{\nu})$ varying from 0.51 to 0.525 depending on photon energy [see *Ndengue et al.*, 2012b, Figure 4]. Similarly, $\phi_{668}(68+6;\tilde{\nu})$ varies from 0.52 to 0.55. The deviation of $\phi_{668}(68+6;\tilde{\nu})$ from 0.5 is about double that of $\phi_{667}(67+6;\tilde{\nu})$, indicating a mass-dependent behavior of these branching ratios.

The photolysis rates of the 667 and 668 isotopologues, $J_{667}(h)$ and $J_{668}(h)$, can be split into two parts corresponding to the two isotopic channels:

$$J_{667}(h) = J_{667}(67 + 6; h) + J_{667}(66 + 7; h) \quad (9)$$

with

$$J_{667}(67 + 6; h) = \int \sigma_{667}(\tilde{\nu}) S(\tilde{\nu}, h) \phi_{667}(67 + 6; \tilde{\nu}) d\tilde{\nu} \quad (9a)$$

and

$$J_{667}(66 + 7; h) = \int \sigma_{667}(\tilde{\nu}) S(\tilde{\nu}, h) \phi_{667}(66 + 7; \tilde{\nu}) d\tilde{\nu}. \quad (9b)$$

Three similar expressions can be obtained for ^{18}O.

The altitude dependences of $J_{667}(66+7;h)$ and $J_{668}(66+8;h)$ (not shown) are very similar (within a factor of 2 for the horizontal axis), with $J_{667}(h)$ and $J_{668}(h)$ displayed in Figure 4 because the two branching ratios are close to 0.5. We prefer to show, in Figure 8, the altitude dependence of the ratios $J_{667}(66+7;h)/J_{667}(h)$ and $J_{668}(66+8;h)/J_{668}(h)$. These ratios have their larger deviations from 0.5 for the high altitudes where the contribution of the Hartley band is dominant.

Figure 8 shows that the photolysis of the 667 isotopologue produces between 50.6% and 51.3% of ^{17}O (between 51.2% and 52.6% for ^{18}O) depending on altitude (the complement being the production of ^{16}O). The two pairs of plateaux, between 0 and 20 km and between 40 and 80 km, correspond to the dominant contributions of the Chappuis band and of the Hartley band, respectively, as shown in Figure 5. The Chappuis band favors for the 66 + 7 dissociation channel (a deviation from the ratio of 0.500) which is twofold weaker

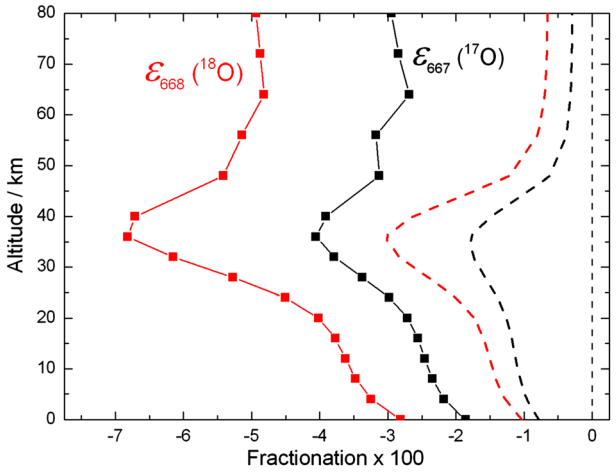

Figure 9. Altitude dependence of the fractionation in ^{17}O (respectively ^{18}O) due to the photolysis of the 667 (respectively 668) isotopologue. The full line + square fractionations are calculated with the $667 \rightarrow 66+7$ (respectively $668 \rightarrow 66+8$) branching ratios of *Ndengue et al.* [2012b]. The dotted lines fractionations are obtained with the branching ratio of 0.5 assumed by *Liang et al.* [2006] (see text).

A similar expression applies for the enrichment in ^{18}O:

$$\varepsilon_{668}\left(^{18}\mathrm{O};h\right) = \left(\left(J_{668}(66+8;h)/\left(J_{668}(h)/2\right)\right) - 1\right). \tag{11}$$

The altitude dependence of these enrichments, ε_{667} (^{17}O; h) and ε_{668} (^{18}O; h), is plotted in Figure 9.

The fractionations shown in Figure 9 depend on both the photolysis isotopic branching ratios, $\phi_{667}(66+7;\tilde{\nu})$ and $\phi_{668}(66+8;\tilde{\nu})$, and on the fractionations, $f_{667}(\tilde{\nu})$ and $f_{668}(\tilde{\nu})$. The relative contributions of the Hartley, Huggins, and Chappuis bands vary strongly with the altitude, as was already shown in Figure 5. Similarly, three ranges of altitude can be distinguished in Figure 9: Below about 20 km, the photolysis rates are dominated by the contribution of the Chappuis band (see Figure 5) which is characterized by a weak fractionation (because the ratios $\sigma_{abc}/\sigma_{666}$ are close to unity); above about 50 km, the photolysis rates are dominated by the contribution of the Hartley band (about 93% ; see Figure 5) which has also a weak fractionation factor; and between about 20 and 50 km, the contribution of the Huggins band to the photolysis rate is significant and this band leads to both a high fractionation and a significant deviation of its branching ratio from 0.5. In order to discriminate between the role of the fractionation factors and the one of the branching ratios, we have plotted in dashed lines the enrichments when the branching ratios are assumed to be 0.5, which is the assumption used by *Liang et al.* [2006]. Note that the dashed enrichments are due solely to the fractionation factors (without any contribution of the branching ratio) which are also at the origin of the isotopologue/isotopomer fractionations plotted in Figure 6. The comparison between the full lines and the corresponding dashed lines shows that the branching ratio contributes for about 50% of the calculated fractionations below 50 km and for up to 85% above this altitude. Between 20 and 50 km the large fractionations (up to −7% for 668 at 36 km) are due to both a large cross-section fractionation $f_{abc}(\tilde{\nu})$ and a large deviation from 0.5 of the branching ratios of the Huggins band. The maximum relative contribution of the Huggins band to the photolysis rate is only of 20% at 28 km (see Figure 5), but this contribution is dominant in terms of fractionations. The calculated fractionations in ^{17}O and ^{18}O due to the photolysis process are significantly higher (almost 3 times higher at 36 km and even more at lower and higher altitudes) than those calculated by *Liang et al.* [2006] and have also slightly different altitude dependences. Liang et al. did not give explicitly the atomic fractionations in ^{17}O and ^{18}O. These fractionations can be derived only from the isotopologue/isotopomer fractionations shown in their Figure 7 if we consider that positive ozone fractionation (a less efficient photolysis) corresponds to a negative fractionation in atomic oxygen liberated during the dissociation. It is important to note, as *Liang et al.* [2006] did, that the calculated fractionations in ^{17}O and ^{18}O can be destroyed by the fast isotope exchange with a bath of atmospheric molecular oxygen before the atomic oxygen reacts with another compound. This isotopic collision exchange, included in a kinetic model like the one used by

than that of the Hartley band. Here it should be noted that the ratios plotted in Figure 8 are mostly dependent on ϕ_{667} $(66+7;\tilde{\nu})$ and ϕ_{668} $(66+8;\tilde{\nu})$. It is interesting to calculate the enrichment (in %) in ^{17}O due to the 667 photolysis which can be approximated by

$$\varepsilon_{667}\left(^{17}\mathrm{O};h\right) = \left(J_{667}(66+7;h)/\left(J_{666}(h)/2\right) - 1\right). \tag{10}$$

Here the front sign is a positive (instead of a negative in equation (2)) because the photolysis of 667 liberates an ^{17}O atom. The factor $\frac{1}{2}$ is due to the fact that each photolysis of 666 produces one ^{16}O atom while the photolysis of 667 can produce either an ^{17}O atom or an ^{16}O atom with approximately the same probability. The enrichment resulting from equation (10) is null if at the same time ϕ_{667} $(66+7;\tilde{\nu}) = 0.5$ and $\sigma_{666}(\tilde{\nu}) = \sigma_{667}(\tilde{\nu})$.

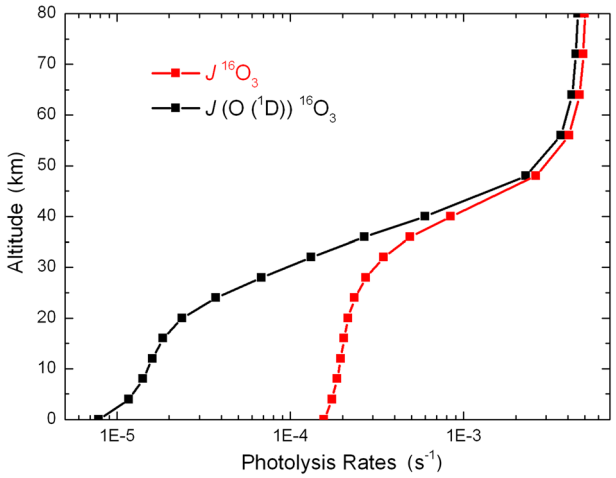

Figure 10. Altitude dependence of J_{666} ($O(^1D)$; h) (noted $J(O(^1D))^{16}O_3$), the rate of production of $^{16}O(^1D)$ by photolysis of the 666 isotopologue. The total photolysis rate, J_{666} (noted $J(^{16}O_3)$), is shown in red for comparison.

Liang et al. [2006], is expected to erase the effect of the fractionation presented in this section. However, in other conditions, it may be important to discriminate between the $O(^1D)$ and the $O(^3P)$ because $O(^1D)$ reacts much faster than $O(^3P)$.

4.2.2. Branching Ratio Between $O(^3P)$ and $O(^1D)$ Atomic Oxygen

Beside the isotope composition of the photolysis products, it is useful to specify the electronic state of the atomic oxygen and the molecular oxygen products because the $O(^1D)$ (an oxygen metastable state) is much more reactive than the $O(^3P)$ (the oxygen ground state). Five electronic channels are energetically allowed for photon energy < 6.2 eV [*Grebenshchikov et al.*, 2007] among which two are spin allowed and three are spin forbidden.

$$O_3 + h\upsilon\left(E_{ph} > 1.05\ \text{eV}\right) \rightarrow O\left(^3P\right) + O_2\left(X^3\Sigma_g^-\right)\ \text{(the triplet channel)} \tag{12}$$

$$O_3 + h\upsilon\left(E_{ph} > 4.00\ \text{eV}\right) \rightarrow O\left(^1D\right) + O_2\left(a^1\Delta_g\right)\ \text{(the singlet channel)} \tag{13}$$

$$O_3 + h\upsilon\left(E_{ph} > 3.01\ \text{eV}\right) \rightarrow O\left(^1D\right) + O_2\left(X^3\Sigma_g^-\right)\ \text{(spin forbidden channel)}. \tag{14}$$

The two other spin-forbidden channels can be neglected in contrast with the one given above because it has been observed experimentally between 3.01 eV and about 4 eV with a branching ratio of 0.0765 [*Sander et al.*, 2011]; see also [*Matsumi and Kawasaki*, 2003]. The branching ratio to this spin forbidden channel has not been calculated, and we have added 0.0765 to each of our calculated branching ratios between 24,330 cm^{-1} and 32,270 cm^{-1}, assuming no isotopologue/isotopomer dependence.

The branching ratio to the singlet channel, $\phi_{666}(O(^1D); \tilde{\nu})$, which depends on the photon energy (or its wavelength), has been calculated with the MCTDH code. Our $\phi_{666}(O(^1D); \tilde{\nu})$ is shown in *Ndengue et al.* [2012b, Figure 6] where it is compared with previous calculations of *Grebenshchikov and Rosenwaks* [2010] and *Schinke and McBane* [2010].

Using our $\phi_{666}(O(^1D); \tilde{\nu})$ and the actinic flux defined above in section 2, we have calculated the $O(^1D)$ rate of formation due to ozone photolysis as a function of the altitude:

$$J_{666}\left(O\left(^1D\right); h\right) = \int \sigma_{666}(\tilde{\nu}) S(\tilde{\nu}, h) \phi_{666}\left(O\left(^1D\right); \tilde{\nu}\right) d\tilde{\nu}. \tag{15}$$

The altitude dependence of J_{666} ($O(^1D)$; h) is shown in Figure 10.

In Figure 10, the decrease of J_{666} ($O(^1D)$; h) is steeper than the one of the total photolysis rate because the part of the actinic flux at $E > 32{,}000\ cm^{-1}$ (which is required to produce $O(^1D)$) decreases faster (with decreasing altitude) than the total actinic flux.

Similar calculations providing $\phi_{abc}(O(^1D); \tilde{\nu})$, the branching ratio to the $O(^1D)$ channel for the other isotopologues noted *abc*, have been performed for the 676, 686, 667, and 668 isotopologues and are shown in *Ndengue et al.* [2012b, Figure 7]. These $\phi_{abc}(O(^1D); \tilde{\nu})$ are very similar, and their tiny differences are probably

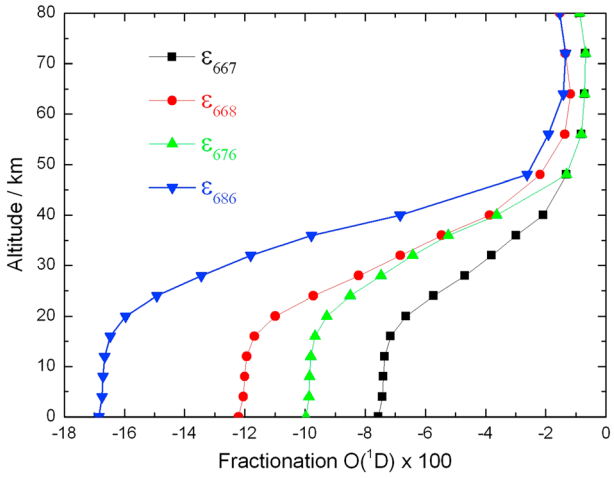

Figure 11. Photolysis contribution to the fractionations in $O(^1D)$ for the four isotopologues, 667, 668, 676, and 686. Globally, the 667, 676, 668, and 686 minor isotopologues produce significantly less $O(^1D)$ (whatever the oxygen isotope) than the main 666 isotopologue.

too weak to be measured experimentally. For most of the applications, the energy dependence of $\phi_{666}(O(^1D);\tilde{\nu})$ can be used for all the isotopologues/isotopomers and the *abc* subscripts can be omitted. Nevertheless, we have calculated the differences between the production rates of $O(^1D)$ by photolysis of the various isotopologues/isotopomers.

For the three symmetric isotopologues, 666, 676, and 686, the photolysis rates split into two parts:

$$J_{abc}(h) = J_{abc}\left({}^{16}O(^1D);h\right) + J_{abc}\left({}^{16}O(^3P);h\right), \quad (16)$$

where

$$J_{abc}\left({}^{16}O(^1D);h\right) = \int \sigma_{abc}(\tilde{\nu})S(\tilde{\nu},h)\phi_{abc}\left(O(^1D);\tilde{\nu}\right)d\tilde{\nu} \quad (17)$$

and

$$J_{abc}\left({}^{16}O(^3P);h\right) = \int \sigma_{abc}(\tilde{\nu})S(\tilde{\nu},h)\left[1-\phi_{abc}\left(O(^1D);\tilde{\nu}\right)\right]d\tilde{\nu}. \quad (17a)$$

For the two asymmetric isotopologues, 667 and 668, the photolysis rates split into four parts corresponding to the two isotopic channels (e.g., 67 + 6 and 66 + 7 for 667) and the two electronic channels as follows:

$$J_{667}(h) = J_{667}\left(67+6;{}^{16}O(^1D);h\right) + J_{667}\left(67+6;{}^{16}O(^3P);h\right) + J_{667}\left(66+7;{}^{17}O(^1D);h\right) + J_{667}\left(66+7;{}^{17}O(^3P);h\right), \quad (18)$$

where

$$J_{667}\left(67+6:{}^{16}O(^1D);h\right) = \int \sigma_{667}(\tilde{\nu})S(\tilde{\nu},h)\phi_{667}(67+6;\tilde{\nu})\phi_{667}\left(O(^1D);\tilde{\nu}\right)d\tilde{\nu} \quad (19a)$$

$$J_{667}\left(67+6:{}^{16}O(^3P);h\right) = \int \sigma_{667}(\tilde{\nu})S(\tilde{\nu},h)\phi_{667}(67+6;\tilde{\nu})\left[1-\phi_{667}\left(O(^1D);\tilde{\nu}\right)\right]d\tilde{\nu} \quad (19b)$$

$$J_{667}\left(66+7:{}^{17}O(^1D);h\right) = \int \sigma_{667}(\tilde{\nu})S(\tilde{\nu},h)\phi_{667}(66+7;\tilde{\nu})\phi_{667}\left(O(^1D);\tilde{\nu}\right)d\tilde{\nu} \quad (19c)$$

$$J_{667}\left(66+7:{}^{17}O(^3P);h\right) = \int \sigma_{667}(\tilde{\nu})S(\tilde{\nu},h)\phi_{667}(66+7;\tilde{\nu})\left[1-\phi_{667}\left(O(^1D);\tilde{\nu}\right)\right]d\tilde{\nu}. \quad (19d)$$

The expressions (18) and (19a) to (19d), which apply to the 667 isotopologue, can be transposed to the 668 isotopologue by replacing all the sevens by eights.

In section 4.2.1 (see equation (9)) the sum of first and second terms of equation (17) is named $J_{667}(67+6;h)$ and the sum of the third and fourth terms is named $J_{667}(66+7;h)$.

Alternatively, the two electronic contributions, $J_{667}(67+6;\ {}^{16}O(^1D);h)$ and $J_{667}(66+7;\ {}^{17}O(^1D);h)$, can be added providing the photolysis rate of 667 corresponding only to the production of $O(^1D)$, whatever the oxygen isotope:

$$J_{667}\left(O(^1D);h\right) = J_{667}\left(67+6;{}^{16}O(^1D);h\right) + J_{667}\left(66+7;{}^{17}O(^1D);h\right). \quad (20)$$

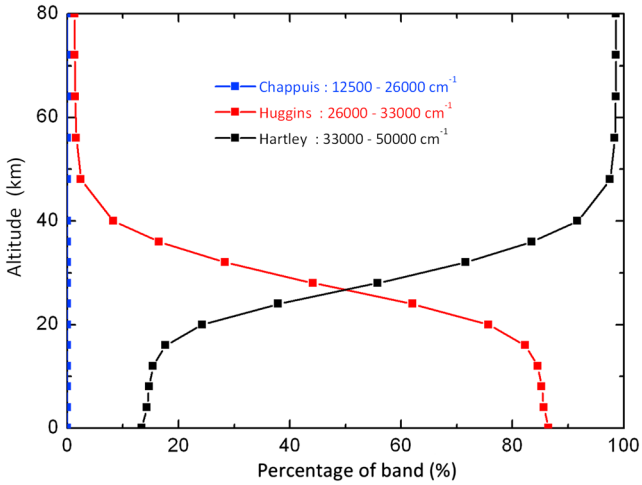

Figure 12. Altitude dependence of the relative contributions (in %) of the Chappuis band (from 12,500 to 26,000 cm^{-1}), Huggins band (from 26,000 to 33,000 cm^{-1}), and Hartley band (from 33,000 to 50,000 cm^{-1}) to the $J_{666}(O(^1D);h)$. The contribution of the Chappuis band is null because of the energy threshold of the $O(^1D)$ channel. The relative contributions for the other isotopologues/isotopomers are very similar and are not shown.

A similar expression can be written for the 668 isotopologue,

$$J_{668}(O(^1D);h) = J_{668}(68+6;^{16}O(^1D);h) + J_{668}(66+8;^{18}O(^1D);h). \quad (21)$$

The rate of production of $O(^1D)$ (then, the O atom can be ^{16}O or ^{17}O or ^{18}O) due to the photolysis of an *abc* isotopologue can be compared to the one of the 666 isotopologue. This comparison can be expressed as an electronic fractionation, analogous to an isotopic fractionation, and defined as follows:

$$\varepsilon_{abc}(O(^1D);h) = \left(\left(J_{abc}(O(^1D);h)/J_{666}(O(^1D);h)\right) - 1\right). \quad (22)$$

Figure 11 shows $\varepsilon_{abc}(O(^1D);h)$, the altitude dependence of the enrichments in $O(^1D)$ for the four monosubstituted isotopologues/isotopomers of ozone.

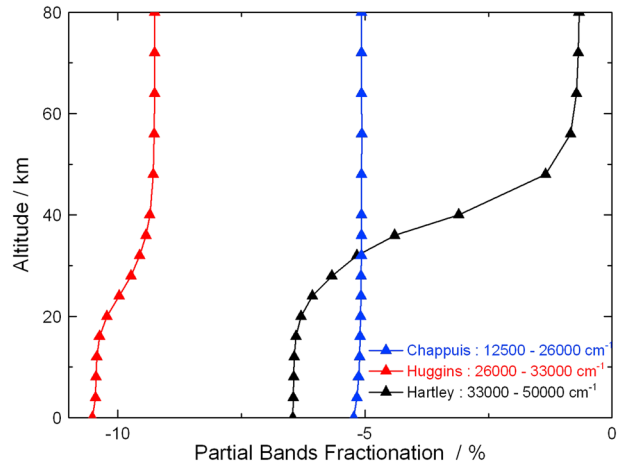

Figure 13. Altitude dependence of the three partial fractionations in $O(^1D)$ due to the photolysis of the 676 isotopologue: Chappuis band (from 12,500 to 26,000 cm^{-1}), Huggins band (from 26,000 to 33,000 cm^{-1}), and Hartley band (from 33,000 to 50,000 cm^{-1}). The partial fractionations in $O(^1D)$ for the other isotopologues/isotopomers (not shown) have a similar altitude dependence and are approximately in the following ratios: $\varepsilon_{686}(O(^1D);h) \approx 2\ \varepsilon_{676}(O(^1D);h)$, $\varepsilon_{668}(O(^1D);h) \approx \varepsilon_{676}(O(^1D);h)$, and $\varepsilon_{667}(O(^1D);h) \approx 0.5\ \varepsilon_{676}(O(^1D);h)$.

The photolysis of the 666, 676, and 686 isotopologues produces only one $^{16}O(^1D)$, while the photolysis of 667 (668) isotopologue produces either one $^{16}O(^1D)$ ($^{16}O(^1D)$) or one $^{17}O(^1D)$ ($^{18}O(^1D)$). The strong (negative) fractionations in $O(^1D)$ shown in Figure 11 at low altitude ($h < 30$ km) are associated to the very low photolysis rates shown in Figure 10 and may be blurred by other processes like collision exchange with O_2.

In order to explain the strong (negative) fractionations of Figure 11, we have calculated the relative contributions (in %) of the three bands (Chappuis, Huggins, and Hartley) to the $J_{abc}(O(^1D); h)$ photolysis rates as a function of altitude. These relative contributions (in %) are rather similar for all the isotopologues, and we have only shown these percents for the 666 isotopologue in Figure 12.

Figure 12 shows that the contribution of the Hartley band is dominant at high altitude, as for the total photolysis rate which is shown in Figure 5. In contrast, at low altitude, the contribution of the Huggins band is dominant for the production of $O(^1D)$. This result differs strongly from the case of total photolysis rate for which the Chappuis band is dominant as shown in Figure 5. The partial enrichments of the three spectral bands (Chappuis, Huggins, and Hartley) to the total enrichments in $O(^1D)$ shown in Figure 11 have been calculated, using equation (15), when the total energy range of integration is divided into the three ranges already used for Figure 12. The results are shown in Figure 13.

Using equation (2b), Figures 12 and 13 explain why, below 20 km, the Huggins band contributes to about 90% of the high enrichments in $O(^1D)$. In contrast, at high altitude, the much weaker enrichments (of the order of 1% for the 676 and 667 isotopologues) are mainly due to the Hartley band. The contribution of the Chappuis band to the $O(^1D)$ enrichments is negligible at all altitudes, in contrast with the enrichments in ozone isotopologues shown in Figure 6 that are dominated by the Chappuis band at low altitude. As already mentioned at the end of the section 4.2.1, the enrichments presented in this section can be destroyed by the collision exchange of atomic oxygen with the bath of molecular oxygen, but this aspect is not treated here.

5. Conclusions and Perspectives

We show that the atmospheric ozone photolysis process contributes significantly to the isotopic fractionations (or enrichments) of the various ozone isotopologues/isotopomers and of the atomic oxygen product. Isotopic budgets of ozone and related compounds should take into account both the formation and the destruction processes of ozone. Here only the contribution of the photolysis process is studied, and the calculated isotopic fractionations are then partial. However, these calculated isotopic fractionations show that the photolysis process plays a significant role and cannot be neglected nor approximated too crudely. A global model is required to predict the overall isotopic enrichments observed experimentally. This model should obviously include the large isotopic effect occurring during the ozone formation process [*Thiemens and Heidenreich*, 1983; *Mauersberger*, 1999; *Janssen et al*., 1999, 2001; *Bhattacharya et al*. [2002]; *Janssen*, 2005; *Mauersberger et al*. [2005]; *Janssen and Tuzson*, 2010], the photolysis processes studied in this paper, and some chemical reactions of ozone with other compounds like O, HO_x, NO_x, CO_2, N_2O, BrO_x, and ClO_x. Such a model has been developed previously by *Ianni* [2002] and by *Liang et al*. [2006], but the photolysis part of the Liang model has three approximations regarding the isotopic dependence of the photolysis process which have been described and discussed in section 4.1.1. These three approximations have now been significantly overcome thanks to the new calculations presented in a series of three previous papers [*Ndengué*, 2010, 2012a, 2012b]. When compared with the previous results of Liang et al., the contribution of the photolysis process to the ozone and atomic oxygen isotope enrichments should be increased respectively by 25% and 50% for the asymmetric and the symmetric isotopologues. Below 25 km, this increase is even larger (mostly because the low-energy part of the Huggins band has been partially neglected by Liang), but this has a moderate impact on the global ozone enrichments because, at low altitudes, the photolysis fractionations remain smaller than the ones of the ozone formation process.

The strong altitude dependence of the isotopologue/isotopomer fractionations presented above (see section 4.1) is mainly related to the altitude dependence of the actinic flux which in turn is strongly related to the altitude dependence of the ozone concentration. Laboratory ozone photolysis experiments can hardly reproduce the photolysis fractionations presented above because these fractionations are strongly dependent on the used light spectrum (e.g., the Hg lamp at 253.65 nm induces very weak fractionation).

To conclude, the comparison of the contributions of the formation and the photolysis processes to the isotopic fractionations (or enrichments) indicates the following:

1. Both of these two processes enrich the minor ozone isotopologues, but their altitude dependences are significantly different: the enrichments due to photolysis have a peak around 35 km, in contrast to the formation process for which the enrichments are predicted to increase monotonically with altitude [*Liang et al*., 2006].
2. The fractionations due to the photolysis process favor the 676 and 686 symmetric isotopologues (they are less destroyed than the 667 and 668 asymmetric isotopologues). This contrasts with the formation process which favors the formation of asymmetric isotopologues [*Janssen*, 2005].
3. The photolysis process is mass dependent in contrast with the formation process which is non–mass dependent [*Thiemens and Heidenreich*, 1983; *Mauersberger*, 1999].

To calculate our enrichments, we have used a single averaged actinic flux depending only on the altitude, as *Liang et al*. [2006] did, because the actinic flux varies considerably with the altitude. Consequently, the fractionations presented above are averaged over the whole Earth (with a latitude cosine weighting). More specific actinic fluxes (e.g., depending on the latitude and/or the season) can be used in order to determine ozone and/or atomic enrichments corresponding to specific geographic situations.

The more promising application of the ozone enrichments is the collisional transfer of its ^{17}O and ^{18}O enrichments to CO_2 [*Wiegel et al*., 2013] and/or N_2O because these molecules have much longer atmospheric lifetimes than O_3 and then are good "integrators" of the ozone oxygen isotope composition which is varying with pressure and temperature and then with time and location.

Acknowledgments
This work was supported by the ANR project "IDEO" (NT09_436466). S.N. acknowledges financial support from the Agence Universitaire de la Francophonie (AUF). H.-D.M. acknowledges financial support by the Deutsche Forschungsgemeinschft (DFG).

References

Anderson, S. M., J. Morton, and K. Mauersberger (1989), Laboratory measurements of ozone isotopomers by tunable diode laser absorption spectroscopy, *Chem. Phys. Lett.*, *156*, 175–180.

Anderson, S. M., D. Hülsebusch, and K. Mauersberger (1997), Surprising rate coefficients for four isotopic variants of $O + O_2 + M$, *J. Chem. Phys.*, *107*, 5385–5392.

Bhattacharya, S. K., S. Chakraborty, J. Savarino, and M. H. Thiemens (2002), Low-pressure dependency of the isotopic enrichment in ozone: Stratospheric implications, *J. Geophys. Res.*, *107*(D23), 4675, doi:10.1029/2002JD002508.

Brasseur, G., and S. Solomon (1984), *Aeronomy of the Middle Atmosphere*, D. Reidel Publishing Company, Kluver Academic Publishers Group, Dordrecht, Holland.

Brion, J., A. Chakir, J. Charbonnier, D. Daumont, C. Parisse, and J. Malicet (1998), Absorption spectra measurements for the ozone molecule in the 350–830 nm region, *J. Atmos. Chem.*, *30*, 291–299.

Chakraborty, S., and S. K. Bhattacharya (2003), Oxygen isotopic fractionation during UV and visible light photodissociation, *J. Chem. Phys.*, *118*, 2164–2172.

Chance, K., and R. L. Kurucz (2010), An improved high-resolution solar reference spectrum for Earth's atmosphere measurements in the ultraviolet, visible, and near infrared, *J. Quant. Spectros. Radiat. Transfer*, *111*, 1289–1295.

Chapman, S. (1930), A theory of upper atmospheric ozone, *Mem. R. Meteorol. Soc.*, *3*, 103–125.

Cole, A. S., and K. A. Boering (2006), Mass-dependent and non-mass-dependent isotope effects in ozone photolysis: Resolving theory and experiments, *J. Chem. Phys.*, *125*, 184,301–184,314.

Dimitrov, A., K. Sepelt, D. Scheffler, and H. Willner (1998), Chemical synthesis of ozone, isotopic labeling, and redistribution, *J. Am. Chem. Soc.*, *120*, 8711–14.

Grebenshchikov, S. Y., and S. Rosenwaks (2010), Ab initio quantum mechanical study of the $O(^1D)$ formation in the photolysis of ozone between 300 and 330 nm, *J. Phys.Chem.*, *114*, 9809–19.

Grebenshchikov, S. Y., Z. W. Qu, H. Zhu, and R. Schinke (2007), New theoretical investigations of the photodissociation of ozone in the Hartley, Huggins, Chappuis, and Wulf bands, *Phys. Chem. Chem. Phys.*, *9*, 1–21, doi:10.1039/b701020f.

Hathorn, B. C., and R. A. Marcus (1999), An intramolecular theory of the mass independent isotope effect for ozone; I, *J. Chem. Phys.*, *111*, 4087–4100.

Haverd, V., G. C. Toon, and D. W. T. Griffith (2005), Evidence for altitude-dependent photolysis-induced ^{18}O isotopic fractionation in stratospheric ozone, *Geophys. Res. Lett.*, *32*, L22808, doi:10.1029/2005GL024049.

Ianni, J. C. (2002), Kintecus. Windows Version 2.80. [Available at www.kintecus.com.]

Janssen, C. (2005), Intramolecular isotope distribution in heavy ozone ($^{16}O^{18}O^{16}O$ and $^{16}O^{16}O^{18}O$), *J. Geophys. Res.*, *110*, D08308, doi:10.1029/2004JD005479.

Janssen, C., and B. Tuzson (2010), Isotope evidence for ozone formation on surfaces, *J. Phys. Chem. A*, *114*, 9709–9719, doi:10.1021/jp1017899.

Janssen, C., J. Guenther, D. Krankowsky, and K. Mauersberger (1999), Relative formation rates of $^{50}O_3$ and $^{52}O_3$ in $^{16}O^{18}O$ mixtures, *J. Chem. Phys.*, *111*, 7179–7182.

Janssen, C., J. Guenther, K. Mauersberger, and D. Krankowsky (2001), Kinetic origin oft he ozone isotope effect: A critical analysis of enrichments and rate coefficients, *Phys. Chem. Chem. Phys.*, *3*, 4718–4721.

Kaiser, J., T. Röckmann, and C. A. M. Brenninkmeijer (2004), Contribution of mass-dependent fractionation to the oxygen isotope anomaly in stratospheric nitrous oxide, *J. Geophys. Res.*, *109*, D03305, doi:10.1029/2003JD004088.

Krankowsky, D., P. Lämmerzahl, K. Mauersberger, C. Janssen, B. Tuzson, and T. Röckmann (2007), Stratospheric ozone isotope fractionations derived from collected samples, *J. Geophys. Res.*, *112*, D08301, doi:10.1029/2006JD007855.

Liang, M. C., G. A. Blake, and Y. L. Yung (2004), A semianalytic model for photo-induced isotopic fractionation in simple molecules, *J. Geophys. Res.*, *109*, D10308, doi:10.1029/2005JD006342.

Liang, M. C., F. W. Irion, J. D. Weibel, G. A. Blake, C. E. Miller, and Y. L. Yung (2006), Isotopic composition of stratospheric ozone, *J. Geophys. Res.*, *111*, D02302, doi:10.1029/2005JD006342.

Madronich, S., and G. Weller (1990), Numerical integration errors in calculated tropospheric photodissociation rate coefficients, *J. Atmos. Chem.*, *10*, 289–300.

Malicet, J., D. Daumont, J. Charbonnier, C. Parisse, A. Chakir, and J. Brion (1995), Ozone UV spectroscopy. II. Absorption cross-sections and temperature dependence, *J. Atmos. Chem.*, *21*, 263–273.

Matsumi, Y., and K. Kawasaki (2003), Photolysis of atmospheric ozone in the ultraviolet region, *Chem. Rev.*, *103*, 4767–79.

Mauersberger, K., B. Erbacher, D. Krankowsky, J. Günther, and R. Nickel (1989), Ozone isotope enrichment: Isotopomer-specific rate coefficients, *Science*, *283*, 370–372.

Mauersberger, K., P. Lämmerzahl, and D. Krankowsky (2001), Stratospheric ozone isotope enrichments-revisited, *Geophys. Res. Lett.*, *28*, 3155–3158.

Mauersberger, K., D. Krankowsky, C. Janssen, and R. Schinke (2005), Assessment of the ozone isotopic effect, in *Advances in Atomic, Molecular, and Optical Physics*, edited by B. Bederson and H. Walter, pp. 1–52, Elsevier, Amsterdam.

Meyer, H.-D., F. Gatti, and G. A. Worth (2009), *Multidimensional Quantum Dynamics: MCTDH Theory and Applications*, Wiley-VCH, Weinheim.

Ndengue, S. A., F. Gatti, R. Schinke, H.-D. Meyer, and R. Jost (2010), Absorption cross section of ozone isotopologues calculated with the Multiconfiguration Time-Dependent Hartree (MCTDH) Method: I. The Hartley and Huggins bands, *J. Phys. Chem.*, *114*, 9855–9863.

Ndengue, S. A., F. Gatti, R. Schinke, H.-D. Meyer, and R. Jost (2012a), Comparison of the Huggins band for six ozone isotopologues: Vibrational levels and absorption cross section, *J. Phys. Chem. A*, doi:10.1021/jp3064382.

Ndengue, S. A., F. Gatti, R. Schinke, H.-D. Meyer, and R. Jost (2012b), Ozone photodissociation: Isotopic and electronic branching ratios for symmetric and asymmetric isotopologues, *J. Phys. Chem.*, doi:10.1021/jp307195v.

Sander, S. P., et al. (2011), *Chemical Kinetics and Photochemical Data for Use in Atmospheric Studies*, pp. 10–6, JPL Publication, Jet Propulsion Laboratory California Institute of Technology, Pasadena, Calif.

Schinke, R. (1993), *Photodissociation Dynamics*, Cambridge Univ. Press, Cambridge.

Schinke, R., and G. C. McBane (2010), Photodissociation of ozone in the Hartley band: Potential energy surfaces, nonadiabatic couplings, and singlet/triplet branching ratio, *J. Chem. Phys.*, *132*, 044,305, doi:10.1063/1.3299249.

Shaheen, R., C. Janssen, and T. Röckmann (2007), Investigations of the photochemical isotope equilibrium between O_2,CO_2 and O_3, *Atmos. Chem. Phys.*, *7*, 495–509.

Thiemens, M. H., and J. E. Heidenreich (1983), The mass-independent fractionation of oxygen—A novel isotope effect and its possible cosmo-chemical implications, *Science*, *219*, 1073–1075.

U.S. Standard Atmosphere (1976), *National Oceanic and Atmospheric Administration (NOAA), National Aeronautics and Space Administration (NASA)*, pp. 241, United States Air Force (USAF) U.S. Government Printing Office, Washington, D. C.

Warneck, P. (1988), *Chemistry of the Natural Atmosphere*, International Geophysics Series, vol. 41, Academic Press, San Diego.

Wiegel, A. A., A. S. Cole, K. J. Hoag, E. L. Atlas, S. M. Schauffler, and K. A. Boering (2013), Unexpected variations in the triple oxygen isotope composition of atmospheric carbon dioxide, *Proc. Natl. Acad. Sci. U. S. A.*, *110*(44), 17,685.

Yung, Y. L., A. Y. Lee, F. W. Irion, W. B. DeMore, and J. Wen (1997), Carbon dioxide in the atmosphere: Isotopic exchange with ozone and its use as a tracer in the middle atmosphere, *J. Geophys. Res.*, *102*(D9), 10,857–10,866.